In Situ Scanning Tunneling Microscopy of Polycrystalline Platinum Electrodes under Potential Control

Copper Electrodeposition and Pyrrole Electropolymerization

Fu-Ren F. Fan and Allen J. Bard*

Department of Chemistry, The University of Texas, Austin, Texas 78712

ABSTRACT

The surface changes of Pt electrodes immersed in solution under potential control were studied by scanning tunneling microscopy. Various structures were observed on a polished, flame-annealed-quenched polycrystalline electrode. Extended cycling of the electrode in 1*M* H_2SO_4 between the regions where an adsorbed oxide film forms and is removed causes significant roughening of the electrode surface. The electrodeposition of copper on polycrystalline Pt and of polypyrrole on a Pt film on mica was also investigated.

The scanning tunneling microscope (STM) allows very high resolution (atomic or near-atomic) examination of the surfaces of conductive or semiconductive substrates (1, 2). Although originally mainly applied to samples in a vacuum or a gaseous environment, this technique has been used to investigate various substrates immersed in aqueous and nonaqueous solutions (3-9). We have further demonstrated the *in situ* study of anodic dissolution of nickel electrodes in sulfuric acid solution under external polarization conditions and open-circuit corrosion of stainless steel in aqueous chloride media (10).

It has long been recognized that electrochemical oxidation-reduction cycling can modify the structure of Pt electrode surfaces (11-13). Vazquez *et al.* first used the STM to investigate *ex situ* (in air) Pt electrode surface roughening by fast, repetitive oxidation-reduction cycles (14). Later, Itaya *et al.* (15a) performed an *in situ* STM measurement on polycrystalline Pt before and after moderate electrochemical activation without potentiostatic control of substrate and tip. We have also examined the topography of different Pt surfaces after different pretreatments in air or in liquids (15b). These latter STM experiments, utilizing a simple two-electrode (substrate and tip) STM configuration, were able to provide structural images as long as the superimposed faradaic currents remained constant over the time scale of the experiment. However, the results are expected to be potential dependent due to faradaic processes, such as dissolution/redeposition, which can change the morphology of the substrate and tip or affect the interfacial tunneling properties. Thus, appropriate control of the electrochemical reactions, both on the substrate and on the tip, by potentiostatic control is important for maintaining a well-defined electrochemical environment for STM measurements. Lustenberger *et al.* (16) and Wiechers *et al.* (17) have recently reported *in situ* STM measurements under potentiostatic control on highly oriented pyrolytic graphite (HOPG) and Au(111) single crystals, respectively. Reports from this laboratory have also demonstrated *in situ* STM study of a HOPG surface and its anodic oxidation under potential control in 0.1*M* H_2SO_4 (18).

An important aspect of *in situ* monitoring of a substrate under potential control is that it allows one to examine the same small area (*e.g.*, 600 × 600Å) of the electrode surface as the electrode is subjected to different treatments. A difficulty with studying surfaces by STM is that only a tiny area is examined in any one scan, and it is difficult to establish what is an example of a representative portion of the surface. This difficulty is compounded by small changes in the tip that can occur with time. Thus, large displacements of the tip between treatments or removal of the sample from the environment (as in *ex situ* studies) prevents one from noting progressive changes of exactly the same area of the electrode by STM.

Film growth by electrodeposition or electropolymerization on various substrates is a convenient and technically important method for modifying electrode surfaces, *e.g.*, for electrocatalysis. Definition of surface structure of these overlayers is crucial to the understanding of the specific physical and chemical properties of the modified electrode. However, there are still only a few *in situ* techniques that are suitable for the study of various growth modes of thin films on electrodes, especially for sub- or monolayer coverage. The unique capability of STM for obtaining structural information at the atomic or near-atomic level makes it ideally suited for the *in situ* studies of these kinds of electrochemical processes on the electrode surface. There have been some demonstrations of the applicability of STM for *in situ* monitoring of electrodeposition of metals on HOPG (19-21) and Au (7a). We report here *in situ* STM monitoring of surface modification of Pt electrodes under potential control by electrochemical oxidation-reduction cycles, electrodeposition of copper, and electropolymerization of pyrrole in aqueous and nonaqueous solutions.

Experimental

Platinum substrates were prepared by the procedures described previously (22-24). Polycrystalline Pt electrodes were polished with successive grades of wet emery paper and then with 5, 1, and 0.25 μm diamond compounds and finally with 0.05 μm alumina. The polished Pt electrodes were then successively sonicated with acetone, methylene chloride, methanol, and Millipore reagent water. These polished Pt samples were then electrochemically cleaned by oxidation-reduction cycling between 1.15 and −0.22V *vs.* SCE in 1*M* H_2SO_4 for 10 min. After rinsing with Millipore reagent water, these cleaned Pt electrodes were then annealed in a gas-oxygen flame near 1100°C for 1h and subsequently quenched in Millipore reagent water saturated with hydrogen.

Electrochemical measurements were performed with a PAR Model 175 universal programmer, a Model 173 potentiostat, and a Model 179 digital coulometer (Princeton Applied Research Corporation, Princeton, New Jersey) or a custom-built bipotentiostat (25), which was also a part of the feedback control circuit for STM measurement. The electrochemical cell consisted of a Pyrex beaker containing a Pt counterelectrode, saturated calomel electrode (SCE) reference electrode, the substrate and an epoxy-coated glass-encapsulated Ir-Pt or Pt ultramicroelectrode as the tip. The sub-μm tip was constructed and etched by procedures reported previously (4) and then coated with epoxy (18b). A well-prepared tip usually would show a steady-state current of less than 0.5 nA in 10 m*M* $Fe(CN)_6^{4-}$/0.5*M* Na_2SO_4 at a scan rate of 100 mV/s (see Fig. 1). The effective radius of the tip was estimated to be less than 0.2 μm and its exposed area, as determined by the steady-state faradaic current, was less than 4.0×10^{-9} cm^2 (26). In underaerated 1*M* H_2SO_4 solution, the measured electrochemical background current was usually less than 50 pA for a bias voltage of 50 mV.

All chemicals were reagent grade and were used without further purification. All aqueous solutions were prepared

*Electrochemical Society Active Member.

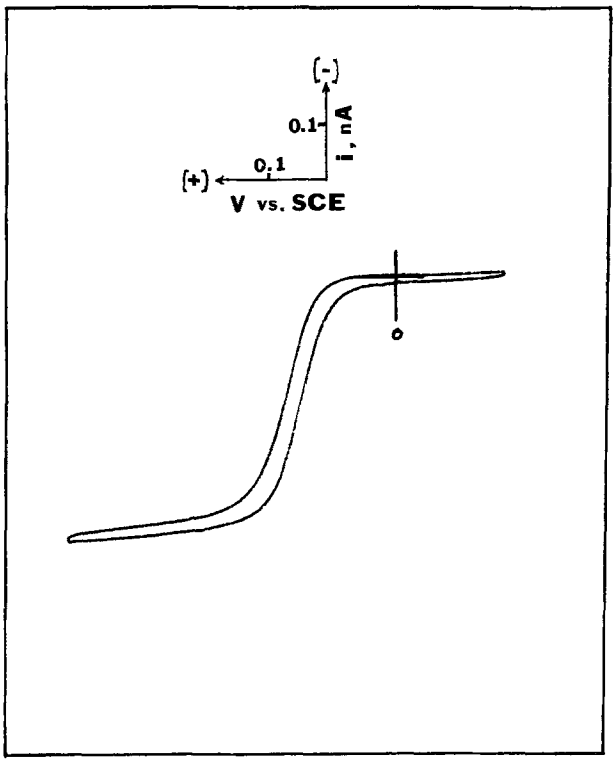

Fig. 1. Cyclic voltammogram with an epoxy-coated glass-encapsulated Ir-Pt ultramicroelectrode tip in 0.5M aqueous Na_2SO_4 solution containing 10 mM $K_4Fe(CN)_6$ at a scan rate of 100 mV/s.

from Millipore reagent water (resistance >18 MΩ). Electrolyte solutions used in the STM measurements were not deaerated, if not otherwise mentioned.

The STM apparatus used here was the same as that reported previously (15). The feedback control electronics are practically identical to those reported, except for the minor difference that the sample is held at virtual ground (via the bipotentiostat) while the tip is held at a selectable potential (also via the bipotentiostat) (Fig. 2). Note that when maintaining the tip at a constant potential where the tip morphology does not change appreciably, any change in the sample potential will yield a change in the tunneling voltage between tip and sample. The STM image of a clean metal surface might not be strongly dependent on tunneling voltage, if it is not too high; however, this might not be true for some materials, such as graphite (27). If not otherwise mentioned, the STM was operated in the constant current mode.

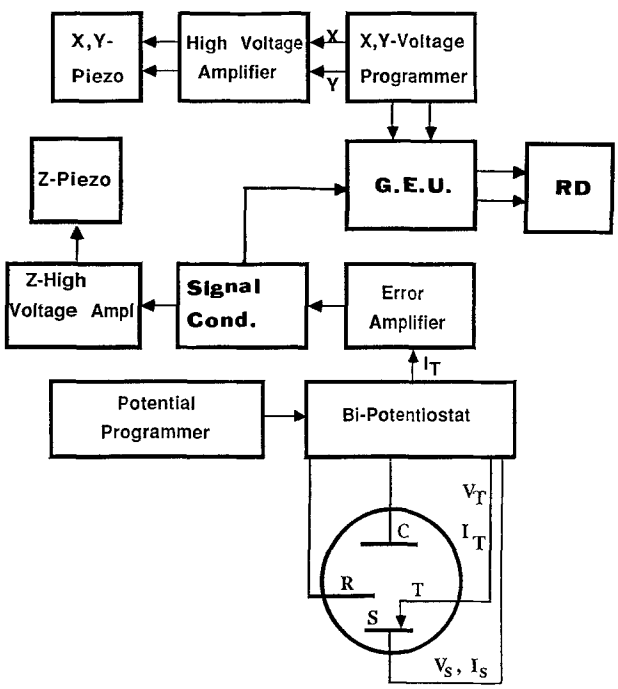

Fig. 2. Block diagram of electronic circuit. C, counterelectrode; T, tip; S, substrate; R, reference electrode; V_s, substrate potential; I_s, substrate current; V_T, tip potential; I_T, tip current; G.E.U., graphics enhancement unit; RD, recorder; signal cond., signal conditioner.

Results and Discussion

STM images of polycrystalline Pt in 1M H_2SO_4.—In Fig. 3 we present a scanning electron microscopy (SEM) micrograph and some STM images of a polished and annealed Pt electrode biased at 50 mV *vs.* tip in 1*M* H_2SO_4. This sample had been prepared as described above and had been repeatedly subjected to electrochemical cleaning-flame annealing cycles. The SEM, as shown in Fig. 3A, indicates that the sample consists of fairly large (a few hundred micrometers) crystal grains. Within each grain, the SEM image shows no unique substructures at a magnification of at least 20,000. However, the STM images at different locations show that different areas of the same sample display fairly different images, although the overall surface imaged is smooth to within 50Å. One structure occasionally observed, as shown in Fig. 3B, consists of fairly regularly spaced mounds, with an average grain size of *ca.* 100-200Å. This hemispherical domain covered an area at least a thousand angstroms wide. Another structure frequently observed is characterized by very flat terraces as shown in Fig. 3C, which are remarkably large, extending over several hundred to a thousand angstroms. The density of large kink sites in this region is quite low. In Fig. 3C, we can barely observe small steps in the middle part of the image. Besides those steps, the surface consists of small corrugations with an amplitude in the range of 1-3Å. These images demonstrate that even for a polycrystalline Pt

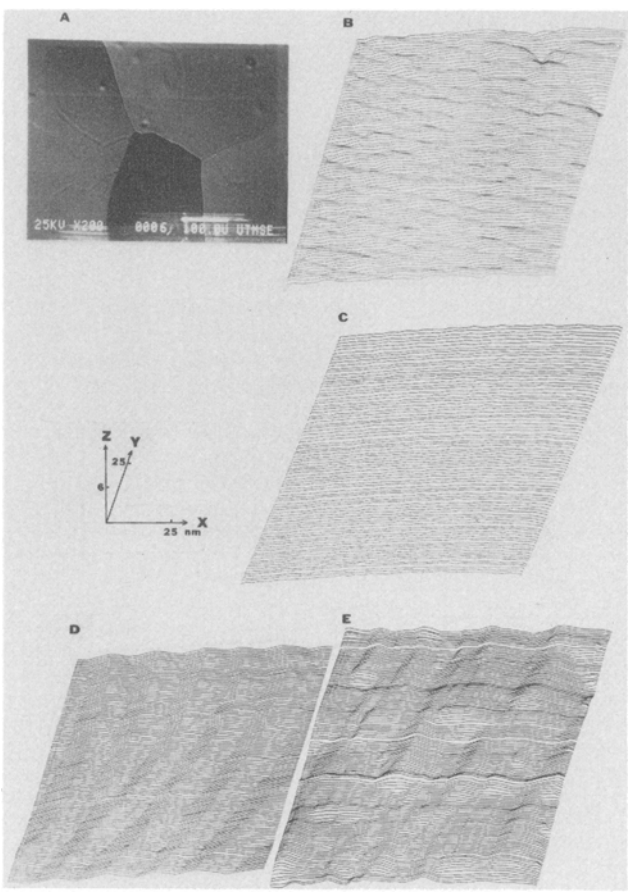

Fig. 3. STM images at different locations of a polycrystalline Pt sample prepared by repeated electrochemical cleaning-flame annealing cycles. The imags were taken in 1M aqueous H_2SO_4 solution at a tunneling current of 0.5 nA and a tunneling voltage (tip *vs.* substrate) of −50 mV. X-rastering rate was 200 Å/s.

sample, the flame treatment can produce some atomically smooth areas, which can extend several hundreds to one thousand angstroms in diameter. Another interesting structure we observed is the textured structure shown in Fig. 3D. The periodic faceting might be formed by polishing a high Miller index plane or by preferential electrochemical etching at a very high aspect ratio, followed by annealing. As shown in Fig. 3D, the periodic surface structures mainly consisted of two crystal faces, which were oriented at an angle close to 160° and separated by *ca.* 200Å. Such periodic surface structures are sometimes seen via high resolution electron microscopy in modulated structures of off-stoichiometry transition metal oxides or slightly misoriented super lattices (28). We have found that the Pt surface images did not change appreciably over prolonged periods of time at rest potential in 1*M* H_2SO_4 in the absence of other species. However, electrochemical oxidation-reduction cycles or bias at potentials where a faradaic process occurs (as demonstrated below) modified the Pt surface dramatically.

In Fig. 4 a sequence of STM images is shown that demonstrates the *in situ* monitoring of surface roughening of Pt electrodes by electrochemical oxidation-reduction cycling in 1*M* H_2SO_4. Before this sequence of experiments was carried out, the STM was allowed to equilibrate thermally with the solution for at least 2h. This minimizes x-y drift in the STM and allows one to examine the same small area (600 × 600Å) of the electrode surface over time. We started with a Pt structure similar to (but slightly noisier than) that shown in Fig. 4A by voltammetric cycling between 1.15 and −0.22V *vs.* SCE. This Pt electrode showed a cyclic voltammogram (CV) as shown in curve 1 of Fig. 5. During the cycling, the tip was left at open circuit and pulled a few hundred angstroms away from the substrate to prevent the possibility of changes of the tip by faradaic dissolution/deposition or other processes. After 5 min cycling at 0.1 V/s, the scanning was stopped at 0.1V *vs.* SCE and the STM image was then taken at rest potential with the tunneling current set at 0.5 nA and tunneling voltage

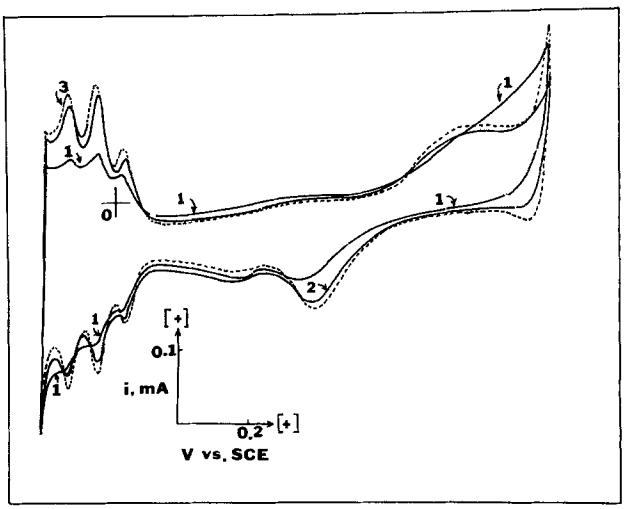

Fig. 5. Cyclic voltammograms of a polycrystalline Pt sample prepared by repeated electrochemical cleaning-flame annealing cycles in 1M aqueous H_2SO_4 solution at scan rate 100 mV/s. 1. Initial scan; 2. after 5 min cycling; 3. after 15 min cycling between −0.22 and 1.15V *vs.* SCE at a scan rate 100 mV/s.

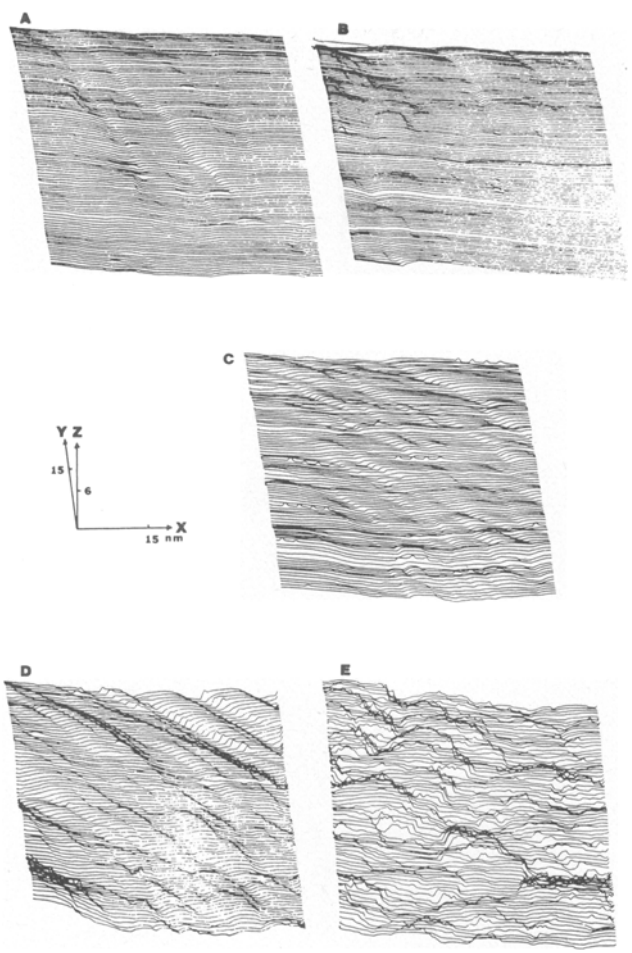

Fig. 4. STM images after different numbers of oxidation-reduction cycles of a polycrystalline Pt sample. The images were taken under the same conditions as those in Fig. 3. A, 5 min cycling between 1.15 and −0.22V *vs.* SCE at 0.1 V/s (*ca.* 20 cycles); B, 15 min cycling; C, 1h cycling; D, 2h cycling; E, 2h cycling but imaged at a different location.

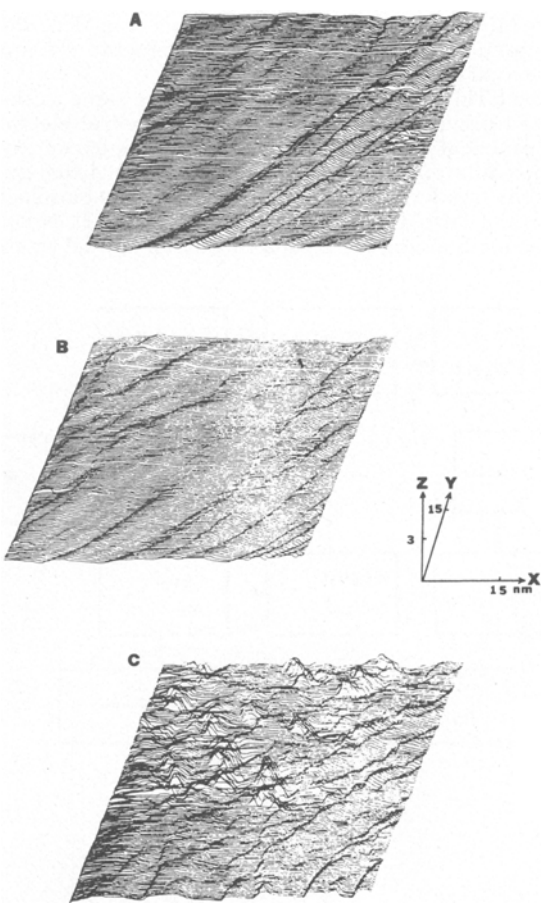

Fig. 6. A sequence of STM images of a polycrystalline Pt sample in 1M aqueous H_2SO_4 solution under potentiostatic control. The tip potential was always biased at 0.10V *vs.* SCE while the substrate potential was biased at A, 0.15V; B, 0.80V; C, 0.15C *vs.* SCE. Each image was taken by allowing *ca.* 15 min equilibration after each change of potential. The residual faradaic tip current was less than 50 pA. The tunneling current was 0.5 nA.

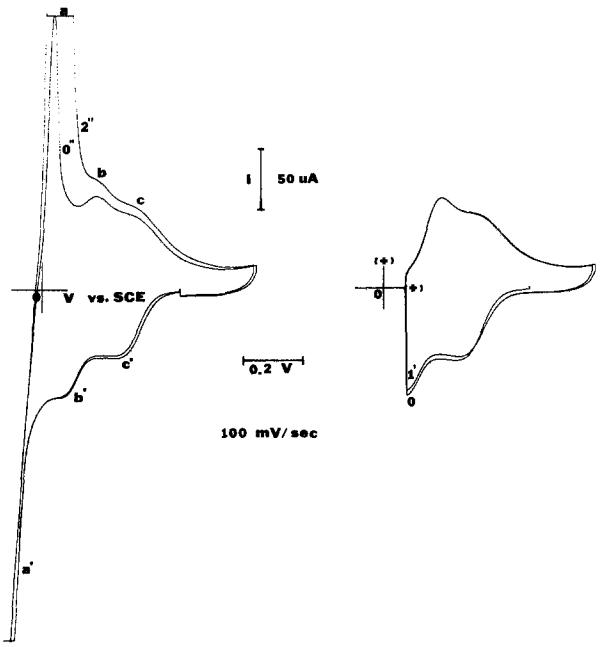

Fig. 7. Cyclic voltammograms of copper deposition and stripping on polycrystalline Pt electrodes in 0.1M $HClO_4$ containing 1 mM $Cu(ClO_4)_2$ at a scan rate of 100 mV/s. The numbers on the curves show the time period of potential hold at the negative limit: 0 and 2s for the left two curves and 0 and 1 min for the two curves shown on the right-hand side.

(tip *vs.* substrate) at −50 mV. The steady-state residual current was less than 10 pA for this tip. After this short period of cycling, the STM image became less noisy and the surface was still quite flat (Fig. 4A). The CV curves (Fig. 5, curve 2) showed that both the hydrogen and the oxygen adsorption/desorption area had increased, perhaps because of the removal of some contamination as indicated by the extra oxidation current occurring before the oxygen evolution region. With further cycling for 15 min (*ca.* 65 cycles), the hydrogen adsorption/desorption area kept increasing (curve 3 of Fig. 5) and some mounds started to appear at the left-hand side of the STM image (see Fig. 4B) while the two steps near the diagonal in Fig. 4A were diminished. As the extent of cycling increased, the ridge structure at the upper-right corner of the images became more and more evident (see Fig. 4B-D). The sequence clearly reveals that the surface of the Pt electrode has progressively roughened by extended electrochemical oxidation-reduction cycling. After 2h cycling (*ca.* 500 cycles), the surface structure was severely modified. As shown in Fig. 4D, a mound structure has been predominantly observed on this area. These long-shaped grains and the ridges at the upper-right corner were oriented in the same direction as the major steps present on the original surface, suggesting that the bulk crystallographic orientation probably has a strong effect on the structure of the surface produced by annealing or by electrochemical redox cycling. Another interesting structure observed at a location different from that for Fig. 4A-D is shown in Fig. 4E, where small isolated and high plateaus with flat tops and steep sides are randomly distributed on the surface. These mesas have terraces ranging from 50 to 200Å in diameter and are several atomic layers high. These results clearly show the restructuring of the Pt surface by potential cycling, which suggests that the Pt atoms regenerated from an oxidized surface in a reduction process do not all return to their original positions. As suggested from the experiments described in the following paragraph, surface Pt atoms probably start to reorganize in the oxide formation region.

In Fig. 6 a sequence of three STM images is shown, which demonstrate changes in surface geometry by controlling the potential of the substrate at a value where a faradaic process is possible; the tip is kept at a potential where no appreciable faradaic reaction takes place during the STM imaging. The Pt electrode and tip were first biased at 0.15 and 0.10V *vs.* SCE, respectively, where there was practically no electrochemical current flowing through either substrate or tip. The residual electrochemical current through the tip was less than 50 pA. As shown in Fig. 6A an imaged area of *ca.* 600 × 600Å exhibits pro-

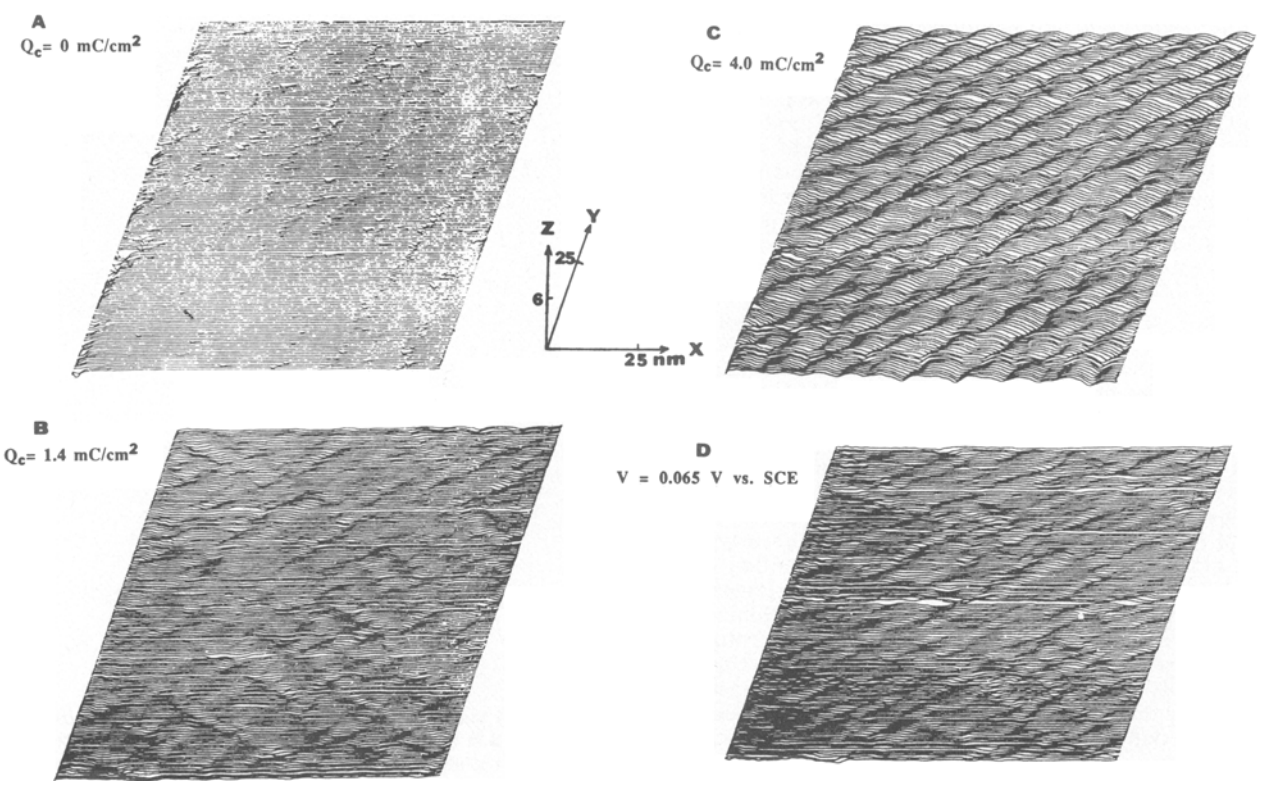

Fig. 8. A sequence of STM images for copper deposition on polycrystalline Pt samples in 0.1M $HClO_4$ containing 1 mM $Cu(ClO_4)_2$. The images were taken in the same solution at a tunneling current 0.5 nA and a tunneling voltage (tip *vs.* substrate) 200 mV. The X-rastering rate was 200 Å/s. A, Bare Pt electrode; B, after deposition of 1.4 mC/cm^2 of Cu; C, after deposition of 4.0 mC/cm^2 of Cu; D, after stripping bulk Cu at 0.065V *vs.* SCE.

nounced ridges and steps of several atoms height, which lie roughly parallel to each other. The upper left-hand side of the surface shows a smoother area. After the imaging, the tip was pulled *ca.* 300Å away from the substrate, and the potential of the substrate was scanned to 0.80V *vs.* SCE and held there while the potential of the tip was maintained at 0.10V *vs.* SCE. No appreciable steady-state tip current was observed. Fifteen minutes later an STM image was taken (substrate potential, 0.80V and the tip potential of 0.10V *vs.* SCE). As shown in Fig. 6B, the surface has been appreciably modified. Corrugations of several atoms height can be clearly observed on the upper-left side, while the middle portions of the neighboring ridges near the diagonal of Fig. 6B decreased, suggesting that the surface structure of the Pt electrode was undergoing rearrangement during the anodic process. Pt surface atoms might move out of their metallic positions, as suggested by Wagner and Ross (29) to accommodate more than a monolayer of oxygen species, forming a disordered surface phase. Note that in contrast to the anodic passivation of Ni (10a) and stainless steel (10b) electrodes, the surface of an oxide-covered Pt electrode is still conductive enough for STM imaging. No indication of the layer of oxygen atoms that exists on the Pt surface at this potential was seen in any STM image.

When the potential of the Pt electrodes was scanned back to 0.15V *vs.* SCE and held there for 15 min, the surface structure was strongly modified. As shown in Fig. 6C, the previously almost linear parallel steps and ridges at the lower right-hand side of Fig. 6A became zig-zag in shape. A number of distinct "islands" of several atoms height, which probably represent newly formed Pt clusters, were clearly seen on the upper-left portion, where the surface structure was modified during the anodic process. These observations suggest that the Pt atoms have undergone substantial transport and rearrangement during the anodic-cathodic potentiostatic control cycle. Since a potential of 0.15V *vs.* SCE does not bring the Pt electrode into a region where either adsorbed or bulk hydrogen is formed, the changes that occur must be attributed to the reaction that removes the adsorbed oxygen-species.

Copper electrodeposition on a polycrystalline Pt substrate.—As shown in Fig. 7 the voltammetric curves for copper deposition and stripping on polycrystalline Pt electrodes in 0.1*M* $HClO_4$ solution containing 1 m*M* $Cu(ClO_4)_2$ were similar to those observed on pyrolytic graphite (30), and show three distinct reduction waves and three corresponding reoxidation peaks. The area under peak a strongly depends on how long the electrode was held at −0.05V *vs.* SCE, while the other two peaks (b and c) do not change with time. This indicates that peak a is related to bulk copper deposition/dissolution. The areas under peaks b and c (and b′ and c′) do not grow after the electrode is held at 0.065V *vs.* SCE for longer than 1s (see the curves shown on the right-hand side of Fig. 7). The peak currents of b, c, b′, and c′ were essentially linearly dependent on the scan rate, suggesting that those peaks represent deposition and dissolution of monolayers or specific active sites or crystal lattice defects. Thus, we identify peaks b′ and c′ as underpotential deposition of Cu on Pt, with peaks b and c representing the corresponding stripping peaks. The wave at a′ and the stripping peak a represent bulk Cu deposition and removal.

Several previous studies of metal deposition with an STM have appeared (7a, 19-21), although these typically did not involve control of the substrate potential. We obtained STM images during a number of independent series of Cu deposition and stripping experiments. Some of the results were ambiguous because of the existing roughness of the surface at the particular locations imaged. However, we usually could observe systematic changes in the topography during Cu deposition. Here, we show one set of our most definitive results to demonstrate the applicability of STM for *in situ* investigation of the early stages of Cu electrodeposition on a polycrystalline Pt substrate. Starting from a nearly atomically flat surface (as shown in Fig. 8A), Cu was electrodeposited on the electrode by biasing it at −0.05V *vs.* SCE where the current was not diffusion-limited. After *ca.* −1.4 mC/cm² of charge had been passed, the current was interrupted before the potential was turned off. To prevent any changes in the tip during the faradaic processes, it was pulled a few thousand angstroms away from the substrate and left at open-circuit condition during electrodeposition.

Assuming that a monolayer of copper atoms arrange as a face-centered lattice on the surface, the 1.4 mC/cm² of charge passed would correspond to *ca.* 3 Cu monolayers (30-33). It appears, as shown in Fig. 8B, that, even for the first several monlayers, copper deposition causes appreciable roughening of the surface, perhaps because it occurs at specific sites rather than as uniform layers. We were not able to observe any uniform adsorbed monolayer or underpotential deposition layer before formation of the larger crystallites. When additional layers of Cu are deposited, as shown in Fig. 8C for the deposition of *ca.* 8 layers of Cu, more clusters are formed with additional roughening of the surface. To observe whether the structure shown in Fig. 8C is related to copper deposition or to a morphological change of the Pt substrate, as described in the previous sections, the substrate was biased at 0.065V *vs.* SCE to strip off the bulk copper layers. The STM image taken after stripping, as shown in Fig. 8D, clearly confirms that the morphology change observed in Fig. 8C is mainly related to Cu deposition. We have attempted to recover the flat surface (image A) by applying a more positive potential (*e.g.*, 0.4V *vs.* SCE) to the substrate, but the surface image

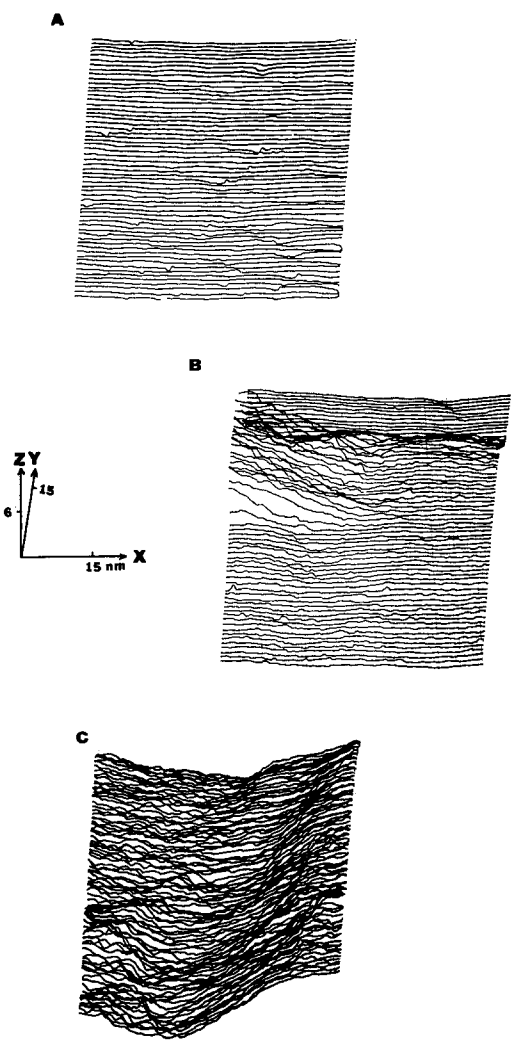

Fig. 9. A sequence of STM images for the electropolymerization of pyrrole on a Pt film (2 μm thick) on a mica substrate in 0.2*M* $TBABF_4$/acetonitrile solution containing 50 m*M* pyrrole. The images were taken in the same solution at a tunneling current of 0.5 nA and a tunneling voltage (tip *vs.* substrate) of −200 mV. X-rastering rate, 500 Å/s. A, Bare Pt electrode; B, after deposition of *ca.* 0.9 mC/cm² of PP; C, after deposition of 3.6 mC/cm² of PP.

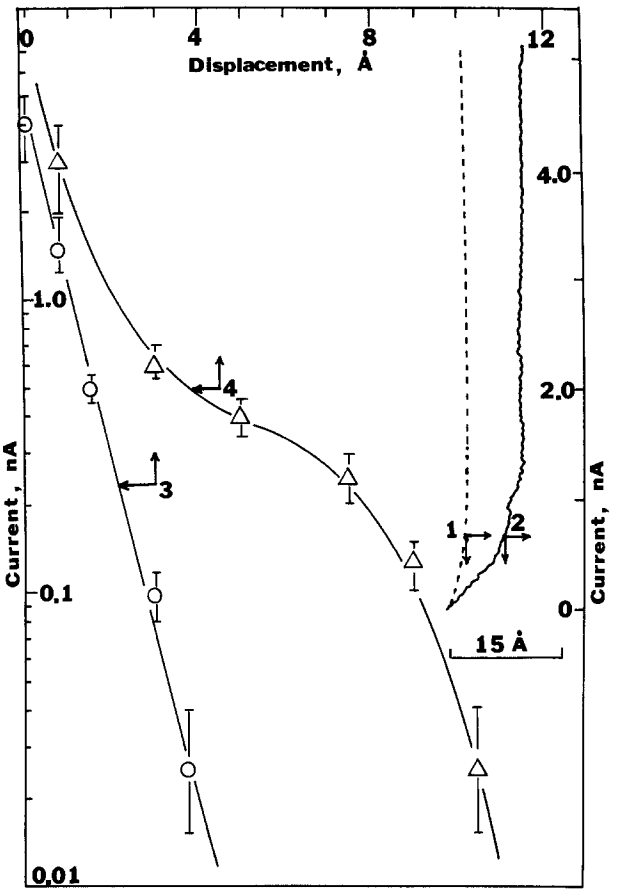

Fig. 10. Tunneling current vs. tip displacement measured in air at tunneling voltage (tip vs. substrate) of −200 mV. 1 and 3, bare Pt electrode; 2 and 4, same sample as used for image Fig. 9C. 1 and 2 are linear scale, whereas 3 and 4 are in semilog scale.

remained essentially the same as Fig. 8D. A control experiment on a Pt substrate in 0.1*M* $HClO_4$ in the absence of Cu^{2+} showed no appreciable surface change after the electrode was biased at −0.05V *vs.* SCE for a period similar to that for Cu deposition and then returned to more positive potentials. These results suggest that a copper deposition and stripping cycle promotes some roughening of the Pt surface.

Electropolymerization of pyrrole on Pt electrodes.—We also investigated the applicability of STM for *in situ* study of the growth of a conductive but deformable substance, such as polypyrrole (PP), in nonaqueous solvent. In Fig. 9 a sequence of three STM images is shown, which illustrates the changes in surface topography of a Pt electrode during electropolymerization of pyrrole in acetonitrile containing 0.2*M* tetrabutylammonium fluoroborate ($TBABF_4$) and 20 to 50 m*M* pyrrole. During electropolymerization, the tip was pulled a few thousand angstroms away from the substrate and left at open-circuit condition. Starting from a fairly flat Pt substrate (*ca.* 2 μm thick layer of Pt sputtered on mica) as shown in Fig. 9A, about 1.2 mC/cm^2 of PP was electropolymerized on the substrate by cycling its potential from 0.2 to 0.9V, back to −0.4V, and finally stopped at 0.2V *vs.* SCE at 100 mV/s. Based on previously reported data (34), the total anodic charge passed, 0.9 mC/cm^2, corresponds to the deposition of a *ca.* 40Å thick layer of PP. The corresponding STM image is shown in Fig. 9B, which clearly shows that PP is not uniformly deposited, but rather shows large structures, such as the one in the upper-left corner of the image. There also appears to be a bundle of strings extending from the left to the right near the top of the image. Figure 9B also exhibits many "ripples" all over the surface, except for the very top region, where PP might not have formed. We suspect that these "ripples" are related to small clusters of PP. As more PP (3.6 mC/cm^2 or *ca.* 150Å) was deposited, the Pt surface was almost fully covered by the polymers and a very different STM image was obtained (Fig. 9C). A noisy and rough surface was clearly seen in image C. The difference in the surface topographs between images A and C is also reflected in a different tunneling current response (i) as a function of displacement (d) (10). For a bare Pt electrode, the current changes by three orders of magnitude within a displacement of *ca.* 4Å (curve 1, Fig. 10) and is exponentially dependent on the distance (curve 3) while for a PP covered Pt electrode, the i *vs.* d curve is noišier and the current initially rises fairly slowly with decreasing distance. As shown in curves 2 and 4 of Fig. 10, a change of *ca.* 10Å is needed to increase i from 0.05 to 1.0 nA, although curve 2 is as steep as curve 1 at very short distances. Note, however, that although the i. *vs.* d curve for a PP-covered Pt electrode is not as steep as that of a bare Pt electrode, it is still much steeper than that for an oxide-covered Ni (10a) or stainless steel (10b) sample. The PP is probably conductive enough to allow its surface to be imaged, but deformation of the PP thin film by the tip may occur during the scan.

Conclusions

The results reported here suggest that STM is a useful technique for the *in situ* study of the physical or electrochemical processes occurring at the electrode/electrolyte interface under potential control. The STM results show that clean and smooth Pt surfaces suitable as STM substrates for electrochemical study can be prepared based on Clavilier's technique. In agreement with *ex situ* studies of morphological changes of Pt surfaces by repetitive oxidation-reduction cycles in acidic solutions, *in situ* STM measurements on annealed polycrystalline Pt electrodes show progressive and preferential etching along the existing defects, although there is not much topographical change at the early stages of cycling (*e.g.*, <10 cycles). The morphology of the Pt surface seems to depend on the potential applied. Surface Pt atoms appear to undergo substantial transport and rearrangement during the anodic-cathodic potentiostatic cycle between the oxide formation and reduction region, even without formation of adsorbed or bulk hydrogen. The electrodeposition of Cu on a polycrystalline Pt substrate before the formation of three-dimensional crystals seems to take place predominantly at specific sites rather than as uniform layers. However, the question whether or not an adsorbed underpotential deposit layer is formed below the clusters cannot be decided at present. There is less doubt that the electropolymerization of pyrrole on Pt in acetonitrile involves formations of clusters on the bare substrate and follows a nucleation-and-growth mechanism rather than a layer-by-layer growth of smooth films.

Acknowledgments

The support of this research by the Office of Naval Research and the National Science Foundation (CHE8402135) is gratefully acknowledged.

Manuscript received Feb. 14, 1989.

The University of Texas assisted in meeting the publication costs of this article.

REFERENCES

1. G. Binnig and H. Rohrer, *Helv. Phys. Acta,* **55,** 726 (1982).
2. G. Binnig and H. Rohrer, *Surf. Sci.*, **126,** 236 (1983).
3. B. Drake, R. Sonnenfeld, J. Schneir, P. K. Hansma, G. Slough, and R. V. Coleman, *Rev. Sci. Instrum.*, **57,** 441 (1986).
4. H.-Y. Liu, F.-R. F. Fan, C. W. Lin, and A. J. Bard, *J. Am. Chem. Soc.*, **108,** 3838 (1986).
5. R. Sonnenfeld and P. K. Hansma, *Science,* **232,** 211 (1986).
6. S. Morita, I. Otsuka, T. Okada, H. Yokoyama, T. Iwasaki, and N. Mikoshiba, *Jpn. J. Appl. Phys.*, **26,** L1853 (1987).
7. (a) R. Sonnenfeld, J. Schneir, and P. K. Hansma, in "Modern Aspects of Electrochemistry," Vol. 19, R. E. White, J. O'M. Bockris, and B. E. Conway, Edi-

tors, Plenum Press, New York, In press; (b) M. M. Dorek, M. J. Heben, N. S. Lewis, R. M. Penner, and C. F. Quate, *ACS Symp. Ser.*, In press.
8. M. M. Dorek, M. J. Heben, C. A. Lang, N. S. Lewis, and C. F. Quate, *Rev. Sci. Instrum.*, **59,** 2333 (1988).
9. S. M. Lindsay and B. Barris, *J. Vac. Sci. Tech.*, **A6,** 544 (1988).
10. (a) O. Lev, F.-R. F. Fan, and A. J. Bard, *This Journal*, **135,** 783 (1988); (b) F.-R. F. Fan and A. J. Bard, *ibid.*, **136,** 166 (1989).
11. (a) F. G. Will, *ibid.*, **112,** 451 (1965); (b) S. Gilman, *J. Electroanal. Chem.*, **9,** 276 (1965).
12. See, for example, P. N. Ross and F. T. Wagner, in "Advances in Electrochemistry and Electrochemical Engineering," Vol. 13, H. Gerischer and C. W. Tobias, Editors, p. 69, John Wiley and Sons, New York (1984).
13. D. Aberdam, R. Durand, R. Faure, and F. El Omar, *Surf. Sci.*, **171,** 303 (1986).
14. L. Väzquez, J. Gómez, A. M. Baró, N. Garcío, M. L. Marcos, J. Gonzalez Velasco, J. M. Vara, A. J. Arvia, J. Presa, A. Garcia, and M. Aguilar, *J. Am. Chem. Soc.*, **109,** 1730 (1987).
15. (a) K. Itaya, K. Higaki, and S. Sugawara, *Chem. Lett.*, **1988,** 421; (b) *J. Phys. Chem.*, **92,** 6414 (1988); (c) F.-R. F. Fan and A. J. Bard, *Anal. Chem.*, **60,** 751 (1988).
16. P. Lustenberger, H. Rohrer, R. Christoph, and H. Siegenthaler, *J. Electroanal. Chem.*, **243,** 225 (1988).
17. J. Wiechers, T. Twomey, D. M. Kolb, and R. J. Behm, *ibid.*, **248,** 451 (1988).
18. (a) A. A. Gewirth and A. J. Bard, *J. Phys. Chem.*, **92,** 5563 (1988); (b) A. A. Gewirth, D. H. Craston, and A. J. Bard, *J. Electroanal. Chem.*, **261,** 477 (1989).
19. R. Sonnenfeld and B. C. Schardt, *Appl. Phys. Lett.*, **49,** 1172 (1986).
20. B. Drake, R. Sonnenfeld, J. Schneir, and P. K. Hansma, *Surf. Sci.*, **81,** 92 (1987).
21. K. Itaya and S. Sugawara, *Chem. Lett.*, **1987,** 1927.
22. J. Clavilier, R. Faure, G. Guinet, and R. Durand, *J. Electroanal. Chem.*, **107,** 205 (1980).
23. M. P. Soriaga and A. T. Hubbard, *J. Am. Chem. Soc.*, **104,** 2735 (1982).
24. J. Clavilier, D. Armand, and B. L. Wu, *J. Electroanal. Chem.*, **135,** 159 (1982).
25. A. J. Bard and L. R. Faulkner, "Electrochemical Methods-Principles and Fundamentals," p. 567, Wiley, New York (1980).
26. R. M. Wightman, in "Electroanalytical Chemistry," Vol. 15, A. J. Bard, Editor, Marcel Dekker, New York (1988).
27. G. Binnig, H. Fuchs, C. Gerber, H. Rohrer, E. Stoll, and E. Tosatti, *Europhys. Letts.*, **1,** 31 (1986).
28. C. N. R. Rao and J. M. Thomas, *Acc. Chem. Res.*, **18,** 113 (1985).
29. F. T. Wagner and P. N. Ross, Jr., *Surf. Sci.*, **160,** 305 (1985).
30. B. H. Vassos and H. B. Mark, Jr., *J. Electroanal. Chem.*, **13,** 1 (1967).
31. N. Furuya and S. Motoo, *ibid.*, **72,** 165 (1976).
32. J. W. Schultze and D. Dickertmann, *Surf. Sci.*, **54,** 489 (1976).
33. S. H. Cadle and S. Bruckenstein, *Anal. Chem.*, **43,** 932 (1971).
34. R. A. Bull, F.-R. F. Fan, and A. J. Bard, *This Journal*, **129,** 1009 (1982).

Scanning Electrochemical Microscopy

High-Resolution Deposition and Etching of Metals

O. E. Hüsser, D. H. Craston, and A. J. Bard*

Department of Chemistry, The University of Texas at Austin, Austin, Texas, 78712

ABSTRACT

Electrochemical methods for the high resolution etching of metals as well as the deposition of metals in polymer films and on conducting substrates are presented. These faradaic processes were carried out with a scanning electrochemical microscope (SECM) (similar in design to the scanning tunneling microscope) and different ionically conducting polymer films such as Nafion, poly(4-vinylpyridine), and poly(bis-(methoxyethoxyethoxide)phosphazene) on the substrate. Continuous patterns of silver, gold, copper, and palladium were deposited, and copper, silver, and gold were etched with widths in the submicron range. The use of polymer-coated substrate electrodes to deposit and etch metals is compared to depositions and etchings performed in electrolyte solutions.

Soon after the introduction of the scanning tunneling microscope (STM) (1, 2) researchers began to investigate the possibility of utilizing it for fabrication. The aim of this work was to take advantage of the high spacial resolution of the STM to produce submicron scale structures. To achieve this goal, a variety of different strategies were employed. For example, metal surfaces were scratched by passing a high current between the STM tip and the metal substrate (3). A similar type of mechanical deformation was achieved by using an STM in the tunneling mode on a silicon substrate coated with a thin film of a metal halide (4). A slightly different approach has been successfully employed, where surfaces were deformed by applying a high-voltage and/or a high local current density (5, 6). McCord and Pease (7,l 8) demonstrated that resist films such as PMMA can be exposed to an electron beam by applying high voltages between the tip and the conducting substrate. A similar method involving plasma deposition of organometallic compounds on the surface of metals has been described by Silver and co-workers (9). Finally, a nonvacuum technique has been described in which semiconductors were photoetched in electrolytes (10) and gold was deposited on gold in a commercially available electroplating solution (11) using a modified STM. More recent reports describing surface modifications with the STM apparatus are mostly based on the ideas previously summarized, with improvements in the resolution obtained, or in application to other material systems.

Recently, in a communication from this laboratory (12, 13), a method was described for the high-resolution deposition of metals in polymer films. This technique is based on the scanning electrochemical microscope (14) (SECM), which is similar in design to the STM. The principle behind this technique is illustrated in Fig. 1 and involves passing a faradaic current between a tip electrode and a metal substrate electrode. A bias voltage is applied between these two electrodes, which are separated from each other by a thin film of an ionically conducting material. The magnitude of the faradaic current that passes through the ionic conductor is kept constant by means of a conventional STM feedback control that monitors the current and adjusts the interelectrode spacing accordingly. By choosing a reasonably low value for this reference current (in the order of nanoamps), the position of the tip electrode can be held so that it is positioned on top of the film with only a very small area actually in contact with the surface. If reducible metal ions are present in the ionic conductor and the tip electrode is poised negative with re-

* Electrochemical Society Active Member.